ACADEMIC PRESS

Available online at www.sciencedirect.com

SCIENCE DIRECT®

Journal of Sound and Vibration 261 (2003) 503–526

JOURNAL OF SOUND AND VIBRATION

www.elsevier.com/locate/jsvi

Simulation of track–ground vibrations due to a high-speed train: the case of X-2000 at Ledsgard

Hirokazu Takemiya*

Department of Environmental and Civil Engineering, Okayama University, Tsushima Naka 3-1-1, 700 8530 Okayama-shi, Japan

Received 15 March 2002; accepted 30 May 2002

Abstract

This paper attempts to demonstrate an application of the author's simulation model for predicting the train-track and nearby ground-borne vibrations by the Swedish high-speed train X-2000 at Ledsgard. The validation of the computation results are tested against the available field measurement data at the site. In this way, the theoretical prediction of the model can be verified whilst also providing a clear-cut explanation of the observed data. The findings are stated as follows:

The train-induced vibrations at the track differ significantly depending on train geometry and speed. At low speeds the response is quasi-static so that the track response due to train axle loads appears mostly downward at the point of their action. On the other hand, at high speeds the train-induced response becomes dynamic due to the inertia generated in the track–ground system, so that the track vibrations appear evenly in both upward and downward directions. As the results of the soft soil deposits at Ledsgard, the high train speed is almost in the trans-Rayleigh wave state so that a large amplified track response appeared due to the resonance between the track behavior and the Rayleigh wave propagation in the ground. This is explained by the frequency–wavenumber spectrum.

To provide useful engineering information relating to vibration mitigation at the train track and nearby ground, a preliminary investigation was carried out by simulating the effect of constructing of a wave impeding barrier (WIB) at the site. The aforementioned frequency–wavenumber spectrum showed that the stiffening effects by the WIB installation into soft layers led a shift of response from a large dynamic one at high train speeds to a small, quasi-static one.

© 2002 Elsevier Science Ltd. All rights reserved.

*Tel./fax: +81-86-251-8146.

E-mail address: e_quakes@cc.okayama-u.ac.jp (H. Takemiya).

0022-460X/03/$ - see front matter © 2002 Elsevier Science Ltd. All rights reserved.
PII: S0022-460X(02)01007-6

1. Introduction

Vibration assessments at and alongside train tracks are becoming of paramount importance as a result of increasing speeds reached by modern trains. The demands for such assessments are twofold: the first is from the viewpoints of train and track stability, and the second is from the environmental problem. The former situation occurs when high-speed trains run over soft track and/or subsoil while the latter concerns the built-up residential and industrial areas. The excessive vibrations produced by high-speed trains have detrimental effects and should be avoided.

Such a case was that of the Swedish National Railway Administration (BANVERKET) which experienced very large track vibrations at Ledsgard on the West Coast Line between Gotenborg and Malmo when they operated the X-2000 train at the high-speed of 200 km/h. In order to investigate the cause of the large vibrations, the BANVERKET carried out field measurement from test runs made at the site. The investigation noted significant differences of response features as train speeds increased. Low-speed operation produced track deformation mostly downwards in a similar way when the train is statically loaded, while high-speed operation led to a significant dynamic response of the track, upward and downward evenly. Furthermore, a significantly large response resulted when the train speed approached the expected Rayleigh wave velocity and just crossed over it. The details of the field tests can be found in Ref. [2].

At this juncture, it might be relevant to provide a brief review of the nature of train-induced vibration and other related topics. A series of impact forces act on the rails at the moment when the train wheels roll over them, with specified time delays occurring according to the train geometry, the sleeper spacing, and the speed of motion. These axle loads are transmitted through the rails to the ballast bed and then into the underlying ground. Depending on the train speed, an inertia force can be generated in the whole track including the ballast bed and embankment, as a result of the dynamics of the track–ground system. The consequence is the wave fields in the whole system, i.e., rail, track and ground. Kenny [3], specifically focusing on the dynamic behavior of the rail–sleeper–ballast system, clarified the track dynamics by using a beam model on the Winkler springs. As a result, he pointed out the existence of a critical wave speed C_{cr} that leads to the track resonance. Dieterman and Metrikine [4] addressed the whole track system comprising rails and ballast bed on the ground, and modelled it by a beam on a half-space. They investigated the change of the behavior by the moving load speed across the Rayleigh wave velocity V_r. but below the Kenny's critical speed C_{cr}.

The wave field generated in a half-space due to a moving surface load was classified by Gakenheimer [5] depending on moving speed c with reference to the shear wave velocity V_s of the ground: the subsonic state for $c<V_s$, transonic state for $V_r<c<V_p$ (P wave velocity), and supersonic state for $V_p<c$. However, Krylov [6,7] proposed the Rayleigh wave speed V_r for the reference speed, so that the sub-Rayleigh state is for the condition $c<V_r$, and trans-Rayleigh state is for the situation where $V_r<c<V_p$. The response at the Rayleigh wave velocity is characterized by a resonance phenomenon. It was thought that such resonance was created at the Ledsgard site because of the soft ground and the high-speed train running.

Train loading is basically a problem of a stationary loading when the speed of motion is assumed to be constant. The train geometry determines the periodic vibration frequencies, while other frequencies originating from the sleeper spacings are also essential. Hence, Krylov [6,7] formulated these frequencies in a unified form. Takemiya et al. [8] replaced the sleeper frequencies

by driving frequencies for the moving loads. The train movement between the negative infinite distance and the positive infinite distance can be formulated by the relative space co-ordinates, with respect to the train movement by the time which elapses. Therefore, we can use the Fourier transform as a solution method. In the transformed domain, the wavenumbers along the direction of train are given by the frequencies divided by the speed of the motion [1,8–11]. This enables us to use the stationary harmonic solution for the dynamic soil–structure interaction. Note however that all frequencies can be involved in the vibration generation from the moving sources. The underlying ground condition determines the resulting vibration and its transmission into the ground. Once the transformed solution is obtained, the inverse Fourier Transform leads the solution in the time domain. Grundmann et al. [12] utilized the Wavelet transform combined with the Fast Fourier transform for an efficient inverse technique.

The vibration prediction for the ground alongside the track depends strongly on ground modelling. If the actual ground has base-rock or stiff supporting sub-soil at a certain depth, it may be modelled using a layered system. Takemiya et al. [8–11]; Sheng et al. [13], Grundmann et al. [12], Kaynia et al. [14] used layered models to predict more accurately the more realistic wave motions. The generation of eigenwaves and their propagation are uniquely characterized by the constituting layer properties of the ground.

The mitigation of track vibrations and of the nearby ground vibrations is also a vital issue. Regarding the X-2000 case, Kaynia et al. [14] investigated the track behavior by increasing the rigidity of the track as a potential remedy. An alternative measure is to improve the soft subsoil beneath the track embankment. Takemiya [9,11] proposed the wave impeding barrier (WIB) procedure for the mitigation of track vibration and proved its effectiveness.

Recently, the author has been able to use the data from the aforementioned X-2000 high-speed train from BANVERKET [2], and this paper attempts to demonstrate the application of the author's simulation model [1] to the case of the X-2000 train. The responses at the track as well as the nearby ground are the main targets of attention. Comparison of the computer simulation and the available data allows us to test the model's predictive capacity while also giving a more effective interpretation of the observed data. The present study focuses on the followings: the periodicity of the source loading from train geometry and speed; the separation of the static and dynamic response components; and the generation mechanism of the nearby ground waves through the track–ground dynamic interaction. The vibration transmission is interpreted in the first instance in the frequency–wavenumber domain. Then, it is interpreted in terms of time histories of displacement, velocity and acceleration for characterizing the vibration propagation with respect to the train speed. Finally, to obtain more information on track response mitigation, a preliminary study was carried out to check the effect of installing WIB in the subsoil beneath the track [9,11]. The effectiveness of the WIB mechanism in reducing vibration is explained using the wave propagation theory.

2. Method of analysis

The formulation described in a previous publication by the author [1] is briefly reviewed at this point and the analysis is then extended to cover the issues of train-track interaction systems.

2.1. The solution method

The Fourier transform method is applied as the solution technique. The Fourier transform pairs are defined for the track or nearby displacement $u(x, y, z)$ as follows:

$$\tilde{\bar{u}}(\xi_x, \xi_y, z, \omega) = \int_{-\infty}^{\infty}\int_{-\infty}^{\infty}\int_{-\infty}^{\infty} u(x, y, z, t)\exp(\mathrm{i}\xi_x x)\exp(\mathrm{i}\xi_y y)\exp(-\mathrm{i}\omega t)\,\mathrm{d}x\,\mathrm{d}y\,\mathrm{d}t, \tag{1}$$

$$u(x, y, z, t) = \frac{1}{8\pi^3}\int_{-\infty}^{\infty}\int_{-\infty}^{\infty}\int_{-\infty}^{\infty} \tilde{\bar{u}}(\xi_x, \xi_y, z, \omega)\exp(-\mathrm{i}\xi_x x)\exp(-\mathrm{i}\xi_y y)\exp(\mathrm{i}\omega t)\,\mathrm{d}\xi_x\mathrm{d}\xi_y\mathrm{d}\omega, \tag{2}$$

where the functions $\bar{u}$ and $\tilde{u}$ represent the transformed displacement with respect to time and space, respectively. The symbol ω is the vibration frequency, ξ_x is the x-directional wavenumber, ξ_y is the y-directional wavenumber, and i stands for an imaginary unit.

The velocity and acceleration responses are obtained from the displacement transform by taking the first and the second derivatives, respectively.

$$\dot{u}(t) = \frac{1}{2\pi}\int_{-\infty}^{\infty}\{\mathrm{i}\omega\bar{u}(\omega)\}\mathrm{e}^{\mathrm{i}\omega t}\,\mathrm{d}\omega, \tag{3}$$

$$\ddot{u}(t) = \frac{1}{2\pi}\int_{-\infty}^{+\infty}\{-\omega^2\bar{u}(\omega)\}\mathrm{e}^{\mathrm{i}\omega t}\,\mathrm{d}\omega. \tag{4}$$

The actual computation of the inverse Fourier transform is carried out by applying the fast Fourier transform algorithm.

2.2. Train loading

Given a moving train consisting of N_t number of cars, the successive axle loading due to the train passage with a constant velocity c at a focused point on the track can be described by

$$P_{N_t}(x - ct) = \sum_{n=0}^{N_t-1} P_n(x - ct + L_n), \tag{5}$$

where

$$L_n = \sum_{e=0}^{n} L_e. \tag{6}$$

The notation L_0 is the distance to a focused position from the first axle load position and L_e $(e = 1, 2, \ldots n)$ is the length of each car. $P_n(x - ct + L_n)$ indicates the nth car's axle loading through the bogies. The detailed expression is

$$\begin{aligned} P_n(x - ct + L_n) = {} & P_{n1}\delta(x - ct + L_n) + P_{n1}\delta(x - ct + a_n + L_n) + P_{n2}\delta(x - ct + a_n + b_n + L_n) \\ & + P_{n2}\delta(x - ct + 2a_n + b_n + L_n), \end{aligned} \tag{7}$$

where P_{n1} and P_{n2} denote the axle loads from the front bogies and from the rear bogies, respectively. The constants a_n and b_n are distances between axles (see Fig. 1). The function $\delta(\cdot)$ stands for the Dirac's delta function. The Fourier transform of Eq. (5) with respect to time and to

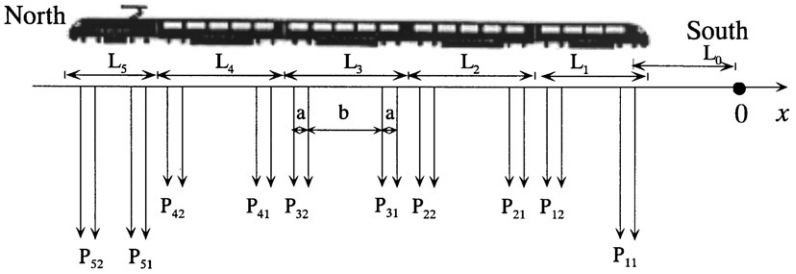

Fig. 1. X-2000 train geometry and axle loads.

the x-co-ordinate leads to the expression

$$\tilde{\tilde{P}}_{N_t}(\xi_x, \omega) = \frac{2\pi}{c}\delta\left(\xi_x - \frac{\omega}{c}\right)\chi(\xi_x), \tag{8}$$

where

$$\chi(\xi_x) = \sum_{n=0}^{N_t-1}[\{P_{n1}(1 + \mathrm{e}^{-\mathrm{i}a_1\xi_x}) + P_{n2}(\mathrm{e}^{-\mathrm{i}(a_1+b_1)\xi_x} + \mathrm{e}^{-\mathrm{i}(2a_1+b_1)\xi_x})\}\exp(-\mathrm{i}\xi_x L_n)]. \tag{9}$$

The contribution from $\xi_x = \omega/c$ is dominant in view of Eq. (8), so that the axle load is characterized in the frequency domain by

$$\chi(\omega/c) = \sum_{n=0}^{N_t-1}[\{P_{n1}(1 + \mathrm{e}^{-\mathrm{i}a_1(\omega/c)}) + P_{n2}(\mathrm{e}^{-\mathrm{i}(a_1+b_1)(\omega/c)} + \mathrm{e}^{-\mathrm{i}(2a_1+b_1)(\omega/c)})\} \cdot \exp(-\mathrm{i}(\omega/c)L_n)]. \tag{10}$$

2.3. Track–ground interaction analysis

A train–track system comprising rails, sleepers and ballast bed is modelled by an Euler–Bernoulli beam. The governing equation under a moving load P_{Nt} at speed c in Eq. (5) is then expressed by

$$EI\frac{\partial^4 u_b}{\partial x^4} + m\frac{\partial^2 u_b}{\partial t^2} + P_b(x, t) = P_{N_t}(x - ct) \tag{11}$$

in which EI is the bending rigidity for the whole train–track system, m is the associated mass per unit length of the system, and $P_b(x, t)$ is the subsoil reaction. The Fourier transform of Eq. (11) with respect to time and space co-ordinate x, leads to

$$\tilde{\tilde{u}}_b(\xi_x, \omega) = \tilde{\tilde{P}}_{N_t}(\xi_x, \omega)H_b(\xi_x, \omega), \tag{12}$$

where $\tilde{\tilde{P}}_{N_t}(\xi_x, \omega)$ is given by Eq. (8) and $H_b(\xi_x, \omega)$ denotes the transfer function of

$$H_b(\xi_x, \omega) = \frac{1}{EI\xi_x^4 - \omega^2 m + \tilde{\tilde{K}}_s(\xi_x, \omega)} \tag{13}$$

with $\tilde{\tilde{K}}_s(\xi_x, \omega)$ defining the subsoil impedance function. In deriving $H_b(\xi_x, \omega)$, the transformed soil reaction $\tilde{\tilde{P}}_b(\xi_x, \omega)$ that makes the counterpart of $P_b(x, t)$ should be obtained first. The formulation is performed on the assumption that the displacement compatibility with the underlying ground at

the center of the track beam, and the force equilibrium over the track width. The result is

$$\tilde{\tilde{P}}_b(\xi_x,\omega)=\tilde{\tilde{K}}_s(\xi_x,\omega)\tilde{\tilde{u}}_b(\xi_x,\omega). \tag{14}$$

It is assumed that the soil reaction along the beam center is distributed transversely over the beam width $2B$ on the surface of layered soils. In the case of a uniform traction distribution, for an approximation, it is defined as

$$\Psi(y)=\begin{cases}1/B, & |y|\leqslant B,\\ 0, & |y|\geqslant B,\end{cases} \tag{15}$$

of which the Fourier transform is given by

$$\tilde{\Psi}(\xi_y)=\frac{\sin(\xi_y B)}{\xi_y B}. \tag{16}$$

The subsoil impedance is then computed from

$$\tilde{\tilde{K}}_s(\xi_x,\omega)=\frac{2B}{\tilde{\tilde{G}}_{zz}(\xi_x,y=0,z=0,\omega)}, \tag{17}$$

where the compliance function matrix $\boldsymbol{G}_s(\xi_x,y,z=0,\omega)$ that includes $\tilde{\tilde{\boldsymbol{G}}}_{zz}(\xi_x,y=0,z=0,\omega)$ for the vertical component is computed from

$$\tilde{\tilde{\boldsymbol{G}}}_s(\xi_x,y,z=0,\omega)=\frac{1}{2\pi}\int_{-\infty}^{\infty}\tilde{\tilde{G}}_s(\xi_x,\xi_y,z=0,\omega)\tilde{\Psi}(\xi_y)\exp(-\mathrm{i}\xi_y y)\,\mathrm{d}\xi_y. \tag{18}$$

Note that $\tilde{\tilde{\boldsymbol{G}}}_s(\xi_x,\xi_y,z,\omega)$ is the three-dimensional wave field Green's function matrix in the wavenumber field of $\xi_x-\xi_y$ for a point load. The relevant elastodynamics is formulated by the stiffness method for a multi-layered ground as discussed in detail in the author's publication [1]. The computation of Eq. (18) is now approximated using the discrete wavenumber method [15].

$$G_{zz}(\xi_x,y,\omega)=\frac{2}{L}\sum_{k=0}^{K}\tilde{\tilde{G}}_{zz}(\xi_x,\xi_{yk},z=0,\omega)\tilde{\Psi}(\xi_{yk})\cos(-\mathrm{i}\xi_{yk}y), \tag{19}$$

where the symmetrical property of the integrand is used. The discrete wavenumbers are given by $\xi_{yk}=2\pi k/L$ with the increment of $\Delta\xi_y=2\pi/L$ based on the fundamental wavelength L appropriate for given frequencies, and K is the total wavenumbers. The time domain solution for the track response is then obtained from the inverse transform of Eq. (2) for Eq. (12). The integral on either ξ_x or ω can be performed analytically in view of Eq. (8), while the remaining integral is carried out by the Fast Fourier transform algorithm.

Once the interaction force $\tilde{\tilde{P}}_b(\xi_x,y=0,z=0,\omega)$ is determined from Eq. (12)–(14), the ground motion vector $\tilde{\tilde{\boldsymbol{u}}}_s(\xi_x,y,z=0,\omega)$ at the location off the track beam is obtained by

$$\tilde{\tilde{\boldsymbol{u}}}_s(\xi_x,y,z=0,\omega)=\left(\frac{2\pi}{c}\right)\tilde{\tilde{\boldsymbol{G}}}_{SSI}(\xi_x,y,z=0,\omega)\chi(\xi_x)\delta\left(\xi_x-\frac{\omega}{c}\right), \tag{20}$$

where $\boldsymbol{G}_{SSI}(\xi_x,y,z=0,\omega)$ represents the transformed Green function of the track–ground system and has the expression of

$$\boldsymbol{G}_{SSI}(\xi_x,y,z=0,\omega)=\tilde{\tilde{\boldsymbol{G}}}_s(\xi_x,y,z=0,\omega)\tilde{\tilde{\boldsymbol{K}}}(\xi_x,\omega)\;H_b(\xi_x,\omega). \tag{21}$$

The response in the space–time domain is computed from the inverse Fourier transform of Eq. (20), resulting in

$$\boldsymbol{u}_s(x,y,z,t)=\frac{1}{2\pi c}\int_{-\infty}^{\infty}\tilde{\tilde{\boldsymbol{G}}}_{SSI}\left(\frac{\omega}{c},y,z,\omega\right)\chi\left(\frac{\omega}{c}\right)\exp\left(\mathrm{i}\frac{\omega}{c}x\right)\exp(-\mathrm{i}\omega t)\,\mathrm{d}\omega. \tag{22}$$

2.4. Effect of sleepers

The train axle loads are transmitted into the ground via sleepers that are assumed to be placed at intervals of distance d along the ballast track. In contrast to the continuous time loading, this discrete time loading gives rise to impulses. However, depending on the rails rigidity and the degree of connection of sleepers to them, the neighboring sleepers react almost in phase [8]. Herein, by applying the related formula by Krylov [6,7], we may replace the train load of Eq. (5) by the following expression for the approximation:

$$P_{N_t}(x-ct)=\sum_{n=0}^{N_t-1}\sum_{m=-\infty}^{\infty}P_n(x-ct+L_n)d\delta(x-md), \tag{23}$$

where the total axle loading integrated over the x-axis is equated to that of the smooth loading in Eq. (5). The Fourier transform by Eq. (23) then becomes

$$\tilde{\tilde{P}}_{N_t}(\xi_x,\omega)=\frac{d}{c}\chi(\xi_x)\sum_{m=-\infty}^{\infty}\exp\left(\mathrm{i}(\xi_x-\frac{\omega}{c})md\right) \tag{24a}$$

or

$$\tilde{\tilde{P}}_{N_t}(\xi_x,\omega)=\frac{2\pi}{c}\chi(\xi_x)\sum_{m=-\infty}^{\infty}\delta\left(\xi_x-\frac{\omega}{c}-m\frac{2\pi}{d}\right). \tag{24b}$$

This indicates that the loading can be approximated by the harmonically oscillating moving load with the driving frequencies $m(2\pi c/d)$, (where $m=$ *integer from* $-\infty$ to ∞), in contrast to the continuous time loading that corresponds to $m=0$ only. The resulting formulation for the track beam dynamics in interaction with the underlying ground is the same as described in Section 2.3. Hence,

$$\begin{aligned}u_s(x,y,z,t)=&\frac{1}{2\pi c}\sum_{m=-\infty}^{\infty}\int_{-\infty}^{\infty}\tilde{\tilde{G}}_{SSI}\left(\frac{\omega+m(2\pi c/d)}{c},y,z\right)\chi\left(\frac{\omega+m(2\pi c/d)}{c}\right)\\&\times\exp\left(-\mathrm{i}\frac{\omega+m(2\pi c/d)}{c}x\right)\exp(-\mathrm{i}\omega t)\,\mathrm{d}\omega.\end{aligned} \tag{25}$$

3. Input data for case study

As noted previously, comprehensive field measurements at different train speeds were conducted by BANVERKET along a train track at Lesgard on the west coast in Sweden. The present simulation is designed to predict the vibration response with respect to train speed at the site, and then to compare the simulation with the measured data by BANVERKET.

Fig. 1 illustrates the Swedish Railway X-2000 high-speed train comprised of five cars. The axle loads at the precise positons on each individual car are taken into account as indicated in Table 1. The track properties are given in Table 2. The site at Ledsgard has a shallow top soil layer over soft clay layers. Field measurement by BANVERKET at the low train speed of 70 km/h shows that the track and ground deformations were small, while at the high train speed of 200 km/h, they were very large, indicating that appreciable non-linear soil behavior had occurred at the soft clay layers. However, the main cause for the large response is the inertia generation as explained later. Based both on the observation and the related indoor experiments, Kaynia et al. [14] interpreted the soil degradation effects as being due to high level strain experienced at high train speed by using the equivalent linear properties model after following an iterative procedure for the concerned strain range. The values of the equivalent linear properties are listed in Table 3 from

Table 1
Train geometry (North bound)

Car number n (Southbound)	5	4	3	3	1
P_{n2}, P_{n1} (kN)	181.5, 180.0	122.5, 122.5	122.5, 122.5	122.5, 122.5	122.5, 122.5
a_n (m)	2.9	2.9	2.9	2.9	2.9
b_n (m)	6.6	14.8	14.8	14.8	11.6
L_n (m)	17.17	24.4	24.4	24.4	22.17

Table 2
Track properties

Train speed	Slow	Fast
Track width, $2B$(m)	3.0	3.0
Mass density, M (t/m)	10.8	10.8
Bending rigidty, EI (MN m^2)	200	80
Damping ratio, β	0.10	0.10

Table 3
Soil parameters used in simulations for train speeds of 70 and 200 km/h (Ref. [14])

Soil layer	Thickness (m)	Mass density (kg/m^3)	Shear velocity V_s (m/s)		Poisson ratio v	Damping ratio β	
			$C = 70$ km/h	$C = 200$ km/h	0.49	$C = 70$ km/h	$C = 200$ km/h
Surface crust	1.1	1500	72	65	0.49	0.04	0.063
Organic clay	3.0	1260 (1380)	41	33 (107)[a]	0.49 (0.45)[a]	0.02	0.058 (0.058)[a]
Clay	4.5	1475	65	60	0.49	0.05	0.098
Clay	6.0	1475	87	85	0.49	0.05	0.064
Half-space	∞	1475	100	100	0.49	0.05	0.060

Note: The values for V_s and β in each column under specified train speed corespond to the equivalent values to be used for the linear analysis.

[a] The values in parentheses indicate the properties after soil improvement (Ref. [16]).

Ref. [14]. The BANVERKET recently conducted a soil stabilization project to the soft portion at the site by injecting lime-cement. However, the details are yet to be published. In this study, based on the author's WIB formula, the expected soil properties are given as averaged values after soil improvement and are also listed in Table 3 [16].

Other parameters used for the present computation work are as follows: the fundamental wavelength in the direction normal to the track is set to L= 2000[m], and the total wavenumbers up to $K = 2000$ are adopted so that we can represent the wave field outwards from the track from the shortest wavelength of 1 m to the longest wavelength of 2000 m. The time increment is set at $\Delta t = 0.005$[s], and the numbers for the Fourier Transform are used up to $N = 2048$, so that we can take into account of frequencies up to 100 Hz and the time durations up to 10 s.

4. Computation results

4.1. Load characteristics

The periodic nature of train load is first investigated. The train geometry, the sleeper spacings and the speed of the motion (that causes the repeated axle loading with time delays), govern the loading frequency characteristics. Although the Southbound direction is considered for the running train at Ledsgard, the train direction is not relevant to the loading frequency characteristics in the Fourier transformed domain. Fig. 2 is the depiction of $\chi(\xi_x)$ from Eq. (9). It may be noted that in view of Eq. (25), the effect of the sleeper impact on vibrations starts to appear in the range of $\xi_x/2\pi > 1$. However, the wavenumber range most important for the track–ground interaction and then the propagation through the ground, is confined to a very low range, $\xi_x/2\pi < 1$ and is explained as follows. In Fig. 2(a), the wavenumber amplitudes are high in the range below 0.1; between 0.3 and 0.48 m^{-1}; and between 0.6 and 0.8 m^{-1} in addition to the large amplitude at zero wavenumber for the static train loading. Since the low wavenumbers become more crucial to the track response, the details for the range $\xi_x/2\pi < 0.2$ are also provided in Fig. 2(b). When the wavenumber representation for abscissa is converted to a frequency representation by the relation $\xi_x = \omega/c$, then we can evaluate the frequency amplitudes for a given train speed.

4.2. Frequency–wavenumber spectrum of the track–ground system

The dynamic characteristic of the track–ground system is described by the transfer function of Eq. (13) in the wavenumber-frequency domain. This intermediate solution of track–ground interaction provides important information not only for understanding of the relevant wave field, but also for utilizing this knowledge to develop the response control measures at the track. A layered soil results in the wave propagation of a dispersive nature. Here, we focus on the response of the track beam first. Fig. 3 shows the contour representation of the frequency–wavenumber spectrum over the most relevant ranges of the variables. We note that the absolute values of the complex transfer function, $|H_b(\xi_x\omega)|$ have peaks that form a "ridge" outwards within a certain value range from the origin. Such features are determined by ground and track beam interaction. At low train speed, the soil properties show a ridge extending almost in a linear fashion on the

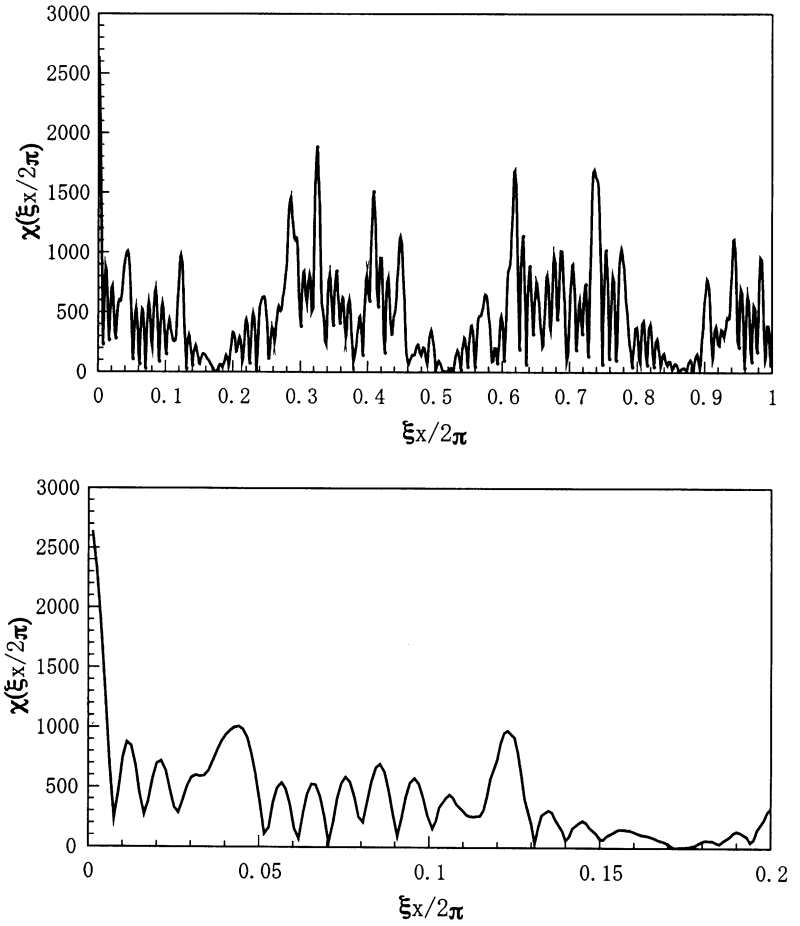

Fig. 2. Axle load characteristic, frequency contents at source: (a) in the range of $\xi_x/2\pi$ below 1.0; (b) close-up in the range of $\xi_x/2\pi$ below 0.2.

spectrum graph, implying a wave field that is less dispersive in nature. The soil properties at high train speed show a spectrum that spreads substantially over the wide wavenumber range even for narrow frequencies, implying a wave field that is very dispersive in nature. The asymptote, which can be read off as roughly 45 m/s for the low strain soil properties and 40 m/s for the high strain soil properties corresponds to the surface wave (generalized Rayleigh wave) propagation speed [16], which is mainly affected by the surface soft soil deposits. This speed specifies the dominant wave propagation at the track site for high wavenumbers and then for high frequencies. Since the slope on the graph defines the speed, the lines corresponding to the train speeds $c = 70, 200$ km/h (or 19.4, 55.6 m/s, respectively) are also drawn in the corresponding figures of Fig. 3. The train speed line for $c = 70$ km/h is located below the ridge. This situation means that the moving train induces almost no wave motions in the ground, so that the track response occurs almost in static, but shifts along the moving train axis by the elapsed time multiplied by the train speed. On the other hand, the speed line for 200 km/h (55.6 m/s) intersects the ridge near its highest peak. Of

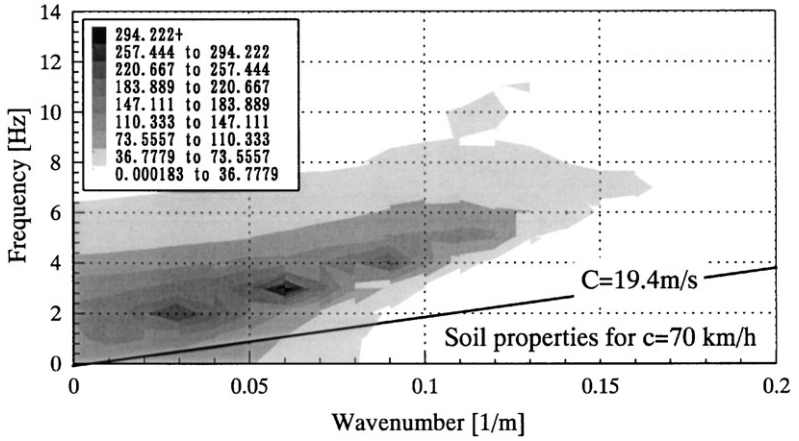

(a) Soil for slow speed, 70 km/h

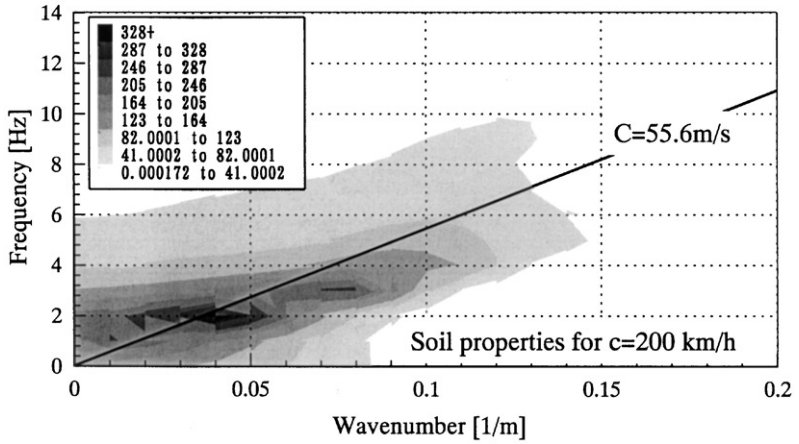

(b) Soil for high speed, 200 km/h

Fig. 3. Frequency–wavenumber spectrum for the ground beneath the track: (a) soil for slow speed, 70 km/h; (b) soil for high speed, 200 km/h.

course, some shift of the ridge position is seen in Fig. 3 due to the soil and beam deteriorations. Therefore, the speed-up of the train is more concerned in the dynamic interaction between ground and track–beam, as explained in what follows.

The cross-sections along the moving speed line is obtained from Eq. (13) by putting $\xi_x = \omega/c$ and is depicted in Fig. 4. The amplitude is seen to change drastically at different train speeds. At the low speed of 70 km/h (19.4 m/s) the response behavior shows a decreasing trend with wavenumber. However, at the high speed of 200 km/h (55.6 m/s), it indicates a clear resonant peak at a specific wavenumber. The value of this wavenumber can be read off as $0.06\,\mathrm{m}^{-1}$ so that by using the relevant formula, the wavelength becomes 16.7 m, and the corresponding frequency is 3.3 Hz. This information, combined with the loading characteristics in Fig. 2, implies a resonance possibility with the surface wave, producing an extraordinarily large track response. Such a

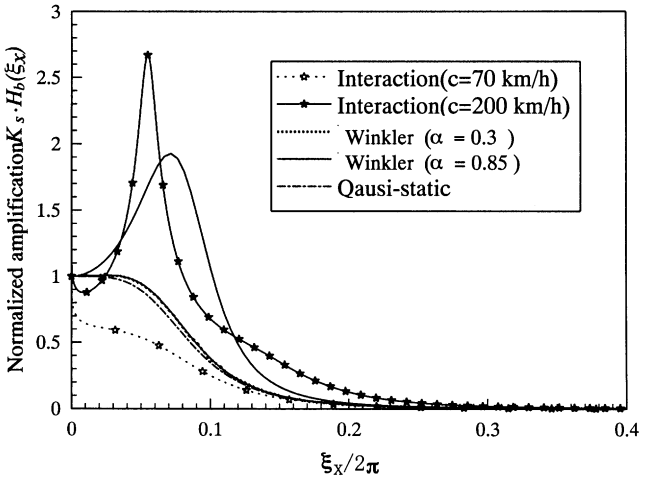

Fig. 4. Frequency transfer functions of track for different train speeds. Comparison with those by Winkler spring model.

phenomenon might actually have occurred when the X-2000 train was operated at 200 km/h at the Ledsgard site.

In the case of the slowly varying ground impedance function $\tilde{K}_s(\xi_x, \omega)$ with the frequency ω, we may approximate it by a constant value K_s. Then, the physical explanation of the track response to the moving load is more simply made by using a beam supported by the Winkler spring. This assumption leads Eq. (13) to

$$H_b(\xi_x) = \frac{1}{K_s(L_c\xi_x^2)^4 - 4\alpha^2(L_c\xi_x^2)^2 + \mathrm{i}8\eta\alpha(L_c\xi_x) + 4}, \tag{26}$$

where $\alpha = c/C_{cr}$ is the speed ratio against the critical speed $C_{cr} = \sqrt[4]{4K_sEI/m^2}$ (the bending wave speed) [3], $L_c = \sqrt[4]{4EI/K_s}$ is the associated wavelength and η is the damping ratio for the critical value. The transfer function multiplied by the Winkler spring constant, $K_sH_b(\xi_x)$, (which is the force action on the ground in the wavenumber expression) is also drawn in Fig. 4 for comparison, based on the assumption that $q = (3\pi/4)L_c = 6.2$ m and $\eta = 0.1$. The quantity q is defined as the major span of static deflection of the track beam under a point load. Once we fix the soil impedance as $K_s = 6.67 \times 10^6$ N/m^2 for $\xi_x = 0$, then $L_c = 6.2$ m is obtained for the track bending rigidity $EI = 80$ MN m^2. The critical speed is derived from Eq. (26) as $C_{cr} = 65$ m for a track mass of 10.8 t/m from Table 2. The moving speed ratio then results in $\alpha = 0.30$ for 70 km/h, and $\alpha = 0.85$ for 200 km/h. Fig. 4 gives the amplification or deamplification depending on the speed ratio. The associated peak location is given by Eq. (26) as $\xi_x/2\pi = \alpha/\left(\sqrt{2}\pi L_c\right) = 0.073$. The corresponding peak value is notably smaller than that from the ground–track interaction analysis, and the peak location is shifted toward the higher wavenumber than the value that is read off in Fig. 4. Therefore, it is concluded that the surface wave propagation in the ground is significantly more important to the track response rather than the critical bending wave propagation in the track. Since the present case satisfies the condition of $\alpha < 1$, the behavior looks like a load transfer function of a single-degree-of-freedom system. For $\alpha < 0.5$, instead of taking the dynamic interaction between the track and the ground, we may use an approximate loading for simplicity,

by taking a static reaction directly on to the ground, dropping the second and third terms in the denominator of Eq. (26). This is indicated in Fig. 4 by the dot-dash line.

From the above investigation, the factors that decrease the speed ratio α to a low value seem to be effective for reducing the track response. In order to increase the critical velocity C_{cr}, alternative solutions are available. One is to increase the track stiffness EI, and the other is to increase the ground stiffness K_s. The former is usually accompanied by an increase of the mass m of the track. Therefore, the latter procedure may be promising in view of the definition of the critical velocity C_{cr}.

4.3. Time domain track response

In theory, the response computation should be rigorously carried out according to Eq. (25). However, as already stated from the frequency–wavenumber spectrum in Fig. 3, it may be sufficient to account for only $m = 0$ in the present case and discard other values of m for which the spectrum field is far outside the range of variables shown in Fig. 3. This justifies taking the smoothly moving axle loads and neglecting the impact of sleepers. Therefore, the response computation is carried out by using Eq. (22) for the Southbound trains. Fig. 5 compares the results of the computation model with the actual field measurements with respect to the displacement at the track for different train speeds. The measured deflections are from the extensometers (displacement sensors at 0–12 m). The model predictions and field measurements fit

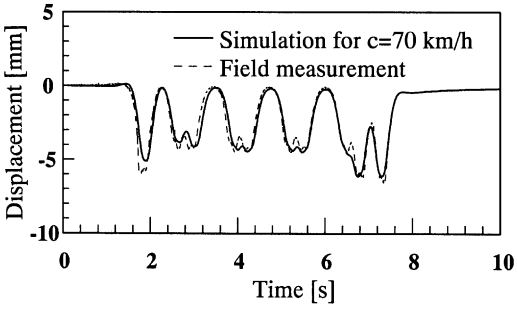

(a) Train speed of 70 km/h, Southbound

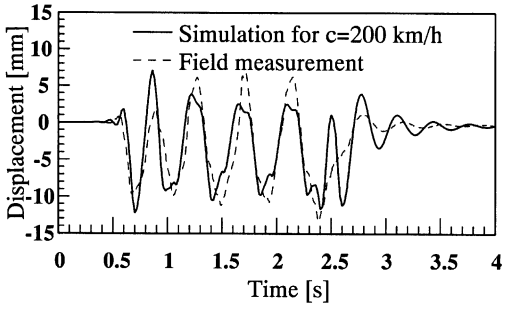

(b) Train speed of 200 km/h, Southbound

Fig. 5. Track beam response for X-2000 train: (a) train speed of 70 km/h, Southbound; (b) train speed of 200 km/h, Southbound.

very closely in the case of the train speed of 70 km/h. The displacement peaks appear at the moment of the passage of respective axle loads at a point under consideration. This means a quasi-static loading state for which only the time delays due to the moving axle loads should be taken into account for the static displacement. However, due to the substantially induced inertia at the track, quite a different response feature appears at the high train speed of 200 km/h, indicating bigger displacements in both positive and negative directions. The difference between the responses at high and low train speeds can be due to the dynamics of the track–ground system.

Fig. 6 shows the Fourier spectrum amplitudes for the displacements shown in Fig. 5. In the case of low train speed, the major contributing frequencies are confined to values below 1 Hz, including a large contribution at zero frequency due to the quasi-static response. The other peaks in Fig. 6 are caused by the train geometry and the train speed. In the case of high train speed, a similar trend exists but significant frequency amplitudes appear around 2.3–2.5 Hz. This is caused by the dynamic effect as can be seen in Fig. 3 where the speed line intersects the ridge of the frequency–wavenumber spectrum in the above frequency range.

In order to give a more precise interpretation to the dynamic response of the track, the ground deflection time histories, when multiplied by train speed, are converted into the deflections along the track. Then we can subtract the converted displacement for the train speed of 70 km/h from that for the train speed of 200 km/h, presumably to derive the purely dynamic component. The result is depicted in Fig. 7(a). The Fourier spectrum of this dynamic component is shown in Fig. 7(b). Due to the impulse loading by train axles on the track, the track–borne bending wave consequently can propagate inside it. The long tail response that shows the track–ground

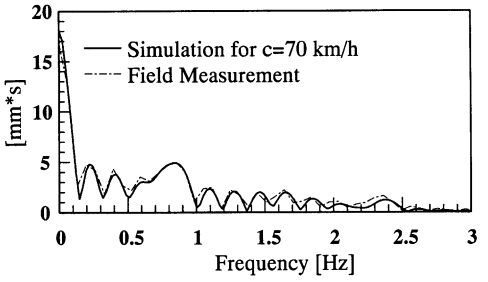

(a) Train speed of 70 km/h, Southbound

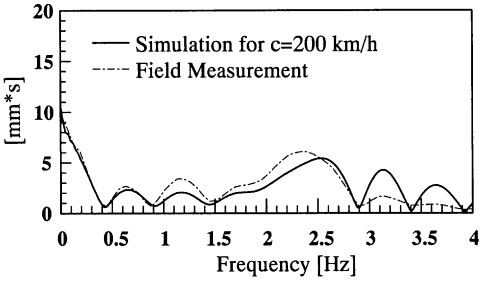

(b) Train speed of 200 km/h, Southbound

Fig. 6. Fourier spectrum of the track response: (a) train speed of 70 km/h, Southbound. (b) train speed of 200 km/h, Southbound.

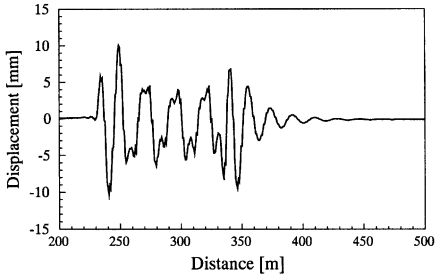

(a) Difference of time histories multiplied by train speed

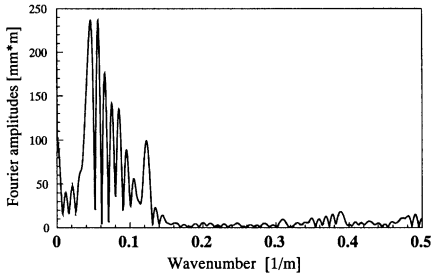

(b) Fourier spectrum amplitude

Fig. 7. Dynamic response from difference between responses for $V = 200$ and 70 km/h: (a) difference of time histories multiplied by train speed; (b) Fourier spectrum amplitude.

characteristic after the train passage at high speed is notable. The predominant wavenumber is observed in the range from 0.04 to 0.1 m^{-1} so that, when the train speed is multiplied, these values result in 2–6 Hz in frequency. This leads to the amplification of such wavenumber band for the train speed of 200 km/h. The initial loading, the drastic change of loading, and the final loading give rise to a very impulsive response that induces the ground borne vibration. The correspondence of the dynamic contribution to the frequency–wavenumber spectrum is clear. The high-speed movement of the load triggers a specific wave field that is determined by its speed and the potential eigenwaves of the track–ground system. This has already been stated in the frequency–wavenumber spectrum of Fig. 3.

4.4. *Vibration transmission from track to nearby ground*

It is also important to assess the vibration transmission from the track to the nearby ground at different train speeds. The nearby ground surface responses can be computed from Eq. (22). In this study, only the vertical component is evaluated. First, the frequency–wavenumber domain spectrum is investigated. The contours of frequency–wavenumber spectrum for displacement are depicted in Fig. 8 for the transverse distances from the track. These spectra correspond to the soil properties for the 70 and 200 km/h train speeds. At the track, the contours from Eq. (13) are identical with those from Eq. (20). Therefore, the spectrum at the track is referred to in Fig. 3. From Fig. 8, it can be seen that at the focused distances from the track (y) the influential zones appear stretched-out from the zero wavenumber to a certain wavenumber on the f–ξ_x plane. In

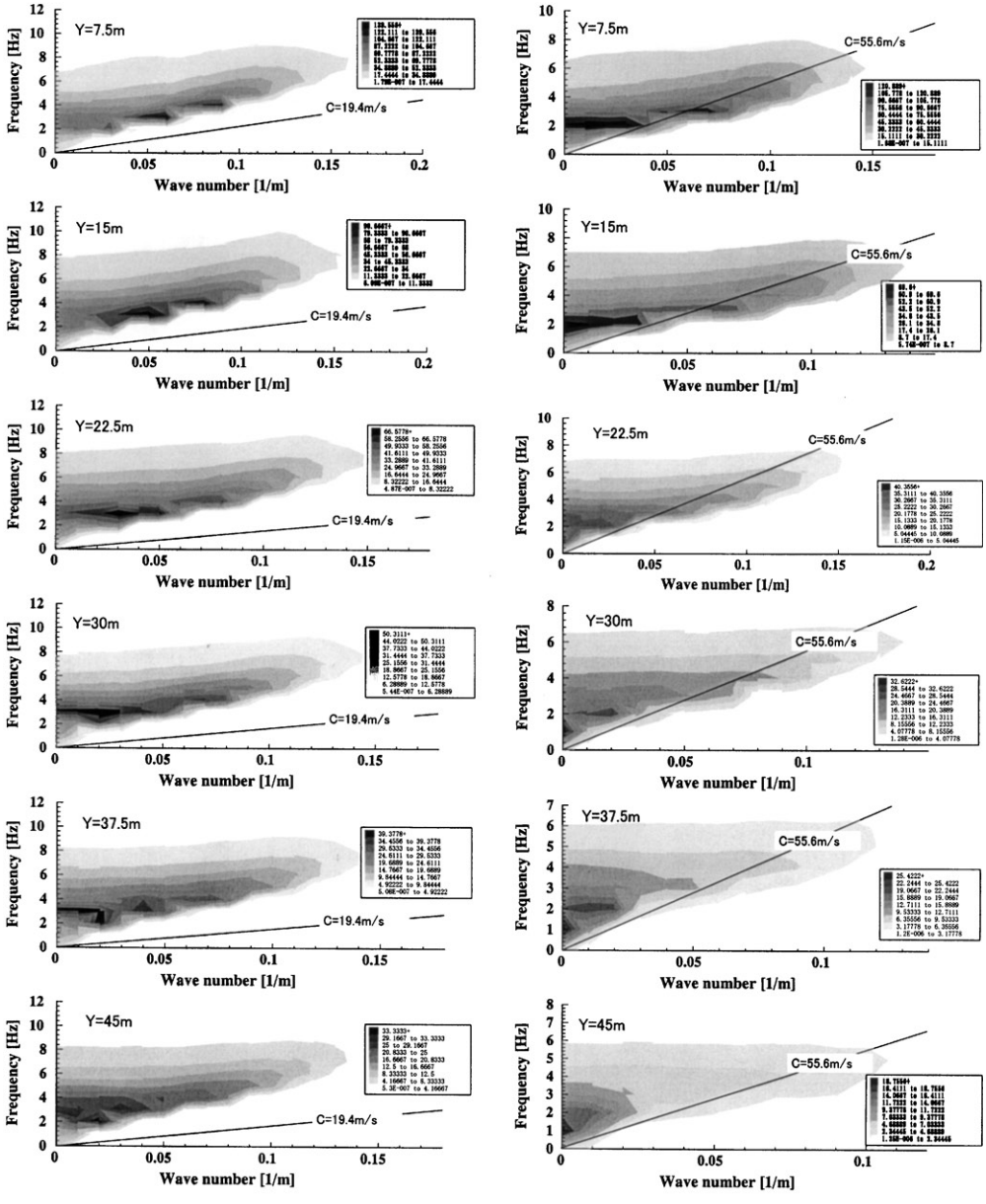

(a) Soil for train speed 70 km/h (b) Soil for train speed 200 km/h

Fig. 8. Frequency–wavenumber spectrum of alongside field of train track: (a) soil for train speed, 70 km/h; (b) soil for train speed, 200 km/h.

contrast to the response contours at the track, for given wavenumbers in Fig. 3, they show the contributing amplitudes only for frequencies higher than those associated with the wavenumbers. In other words, given the frequencies, the wavelengths longer than those associated do not exist.

This reflects the wave cutoff phenomenon due to the soil layering, providing a clear demarcation of the zones for wave propagation or non-propagation. As the distance for the observation from the track is increased, the location of the spectrum ridge shrinks towards the zero wavenumber, while the peak frequency moves slightly towards the lower frequency. In Fig. 8 the train speed lines are also drawn. Note that in the case of a train speed of 70 km/h, the speed line lies far below the wave propagation zone, which means no wave propagation in the rigorous sense. However, in the case of a train speed of 200 km/h, the speed line passes through the wave propagation zone, which means that the wave propagation exists in the true sense.

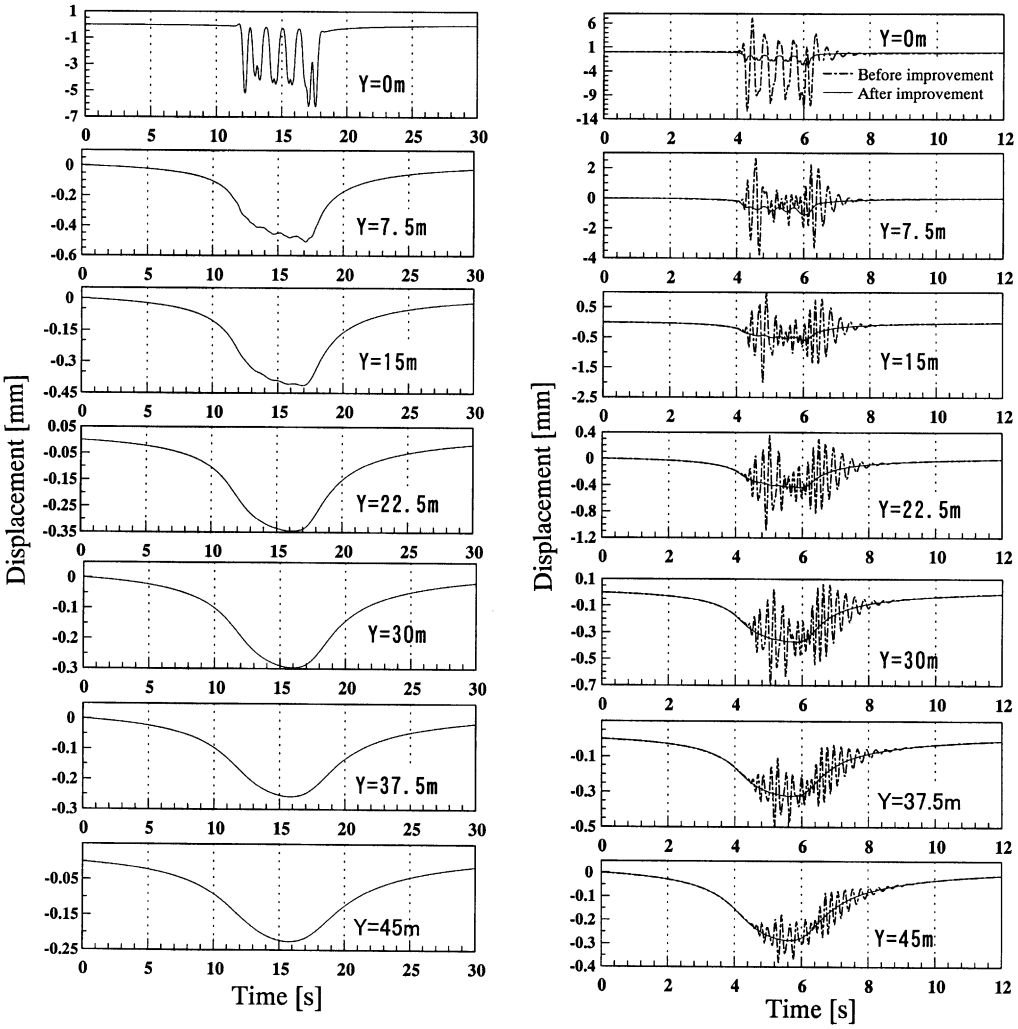

(a) Train speed 70 km/h

(b) Train speed 200km/h, before and after the soil improvement beneath the track

Fig. 9. Displacement response time histories at track and nearby ground surface at train speed before and after the soil improvement beneath the track: (a) 70 km/h; (b) 200 km/h.

The time histories from the inverse Fourier transform are depicted in Fig. 9. For the train speed of 70 km/h, as the focused points are moved outwards from the track, the response features change significantly. In contrast to the response at the track, the displacement at the observation point away from it, say at 7.5 m, shows small fluctuations on a long-span "bowl-shaped" response. The bowl-shaped response is interpreted as a resultant response due to the total train weight while the former small oscillations are associated with the times of arrival of the effect of individual axle loads. They become negligibly small, say 15 m at a distance from the track, and disappear gradually beyond this point, so that only the bowl-shape displacement due to the resultant train load is left. At the observation points farther from the track, the response starts to rise earlier than at the track point due to the quasi-static stress transfer in the ground of the moving total train load. For the train speed of 200 km/h, on the other hand, inertia is induced in the track, and the vibrations are propagated outwards much farther distance from the track. The response appears in the form of vibrations of shorter periods than those at the track that are superimposed on a bowl-shape response of a long period as the distance increases. The bowl-shape response component also occurs for the high-speeds as well as for the slow train speed of 70 km/h. Different predominant frequencies are observed between track and nearby ground, which are in the range of 2–3 and 3–6 Hz, respectively. This is interpreted by reference to Fig. 8 as follows. At the track, the crossing of the spectrum ridge by the train speed line occurs in the frequency range of 2–3 Hz, while at nearby ground it occurs in a wider range of 3–6 Hz. Those crossings determine the ground response features.

The velocity responses are drawn in Fig. 10. The track velocity for the train speed of 70 km/h just follows the quasi-static displacements for successive axle loads. At the ground away from the track, the velocity gradually increases and then decreases following the bowl-shape soil displacement in Fig. 9 due to the resultant trainloads. For the train speed of 200 km/h, on the other hand, the ground velocity is significantly characterized by the dynamic component under individual axle loads. The Fourier transforms of the velocity responses are depicted in Fig. 11. At the track, the wave motions have a predominant frequency at 2.2 Hz and then spread-out over to several Hz, as predicted from the spectrum ridge in Fig. 3. As the distance of the observation from the track increases, the response frequencies are shifted so as to concentrate in the range from 4 to 7 Hz. The spectrum in Fig. 8 substantiates this trend. To check the accuracy of the simulation model, the frequency responses generated by the model are compared with the measurement data obtained at the Ledsgard site. Here, the data from the train track are the time-integrated velocity from the acceleration records. The data at other observation points are directly obtained from the velocity measurement by the geophones. The sensor placed at 7.5 m off the track has a 4.5 Hz high-pass filtering effect, while those at farther distances have 2.0 Hz high-pass filtering. It is noted that a good matching is attained between simulation and measurement, except at 7.5 m distance because of the above sensor characteristic.

The next investigation addresses the acceleration response of the track and the nearby ground for the train speed of 200 km/h only since the low train speed of 70 km/h is quasi-static as already explained. The results are shown in Fig. 12(a). The acceleration time histories at the track ($y = 0$) and those at the ground ($y = 7.5$–45 m) differ appreciably in appearance, and those at the ground keep almost the same waveform, while the amplitudes are reduced with distance. This is presumably because of the high frequencies in the range of 4–7 Hz of a less dispersive nature in the predominant acceleration waves.

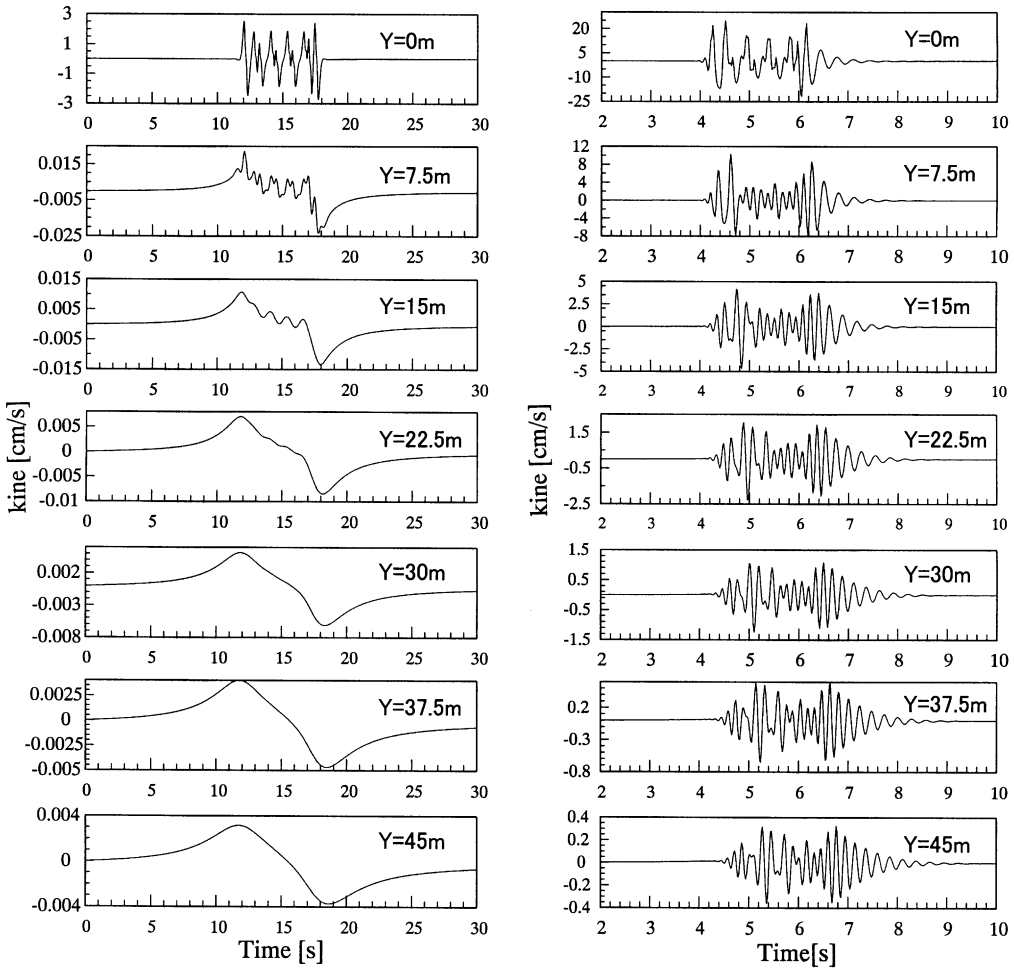

Fig. 10. Velocity response time histories at track and nearby ground surface at train speed: (a) 70 km/h; (b) 200 km/h.

The environmental vibration assessment in Japan is regulated to use the vibration level whose formula is specified as

$$VAL = 20 \log_{10}(A/A_0) \text{ (d}B\text{)} \tag{27}$$

in which A is the acceleration in the unit of m/s^2 and the quantity A_0 is a normalization value of $A_0 = 10^{-5}$ (m/s^2). From the maximum values for different train speeds, the VAL values can be obtained, and are shown in Fig. 13. From an environmental standpoint a critical value is specified beyond which some countermeasure must be taken. For the Shinkansen line in Japan, the regulated value is 70 dB.

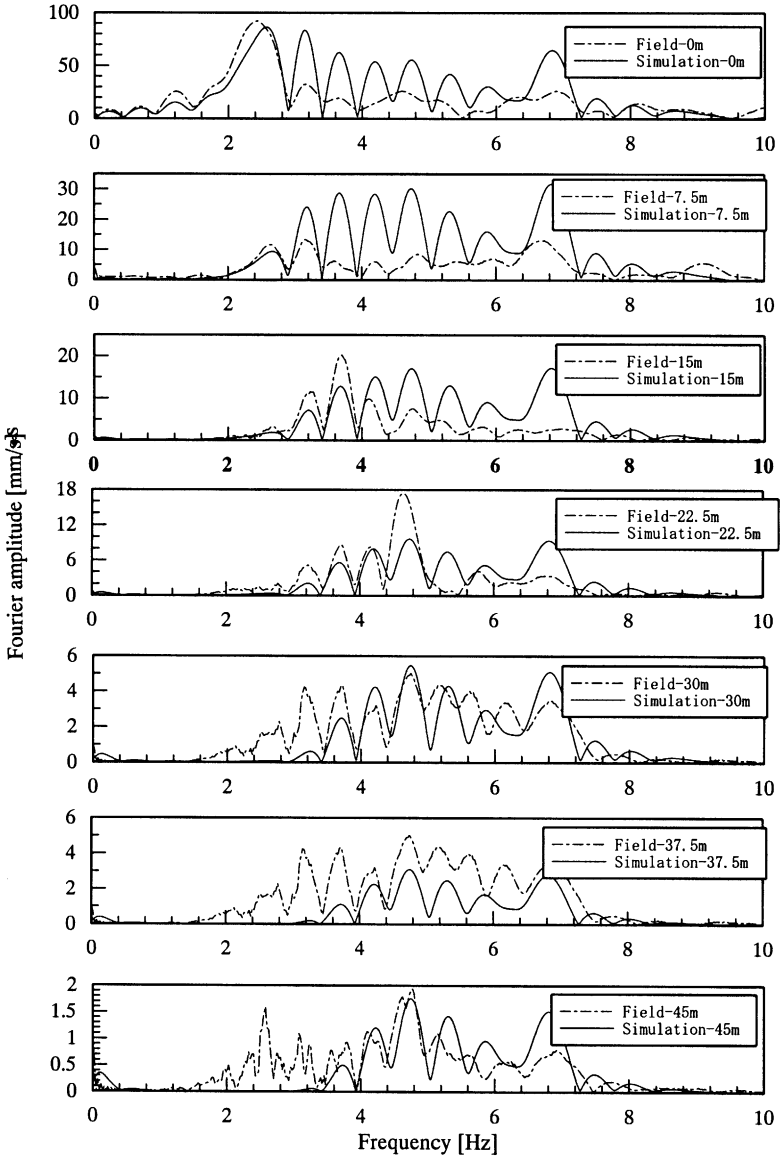

Fig. 11. Fourier spectrum of velocity response at ground surface alongside track. Comparison between simulation and measurement, train speed $c = 200$ km/h

4.5. *Vibration mitigation*

Regarding the reduction of train-induced ground vibrations, the author proposed a promising measure called WIB and X-WIB by use of soil improvement techniques such as injecting cement into the ground. Under the given loading and soil condition, the design of the procedure is specified for the width and depth along train tracks. The author's publications [9,11] can be

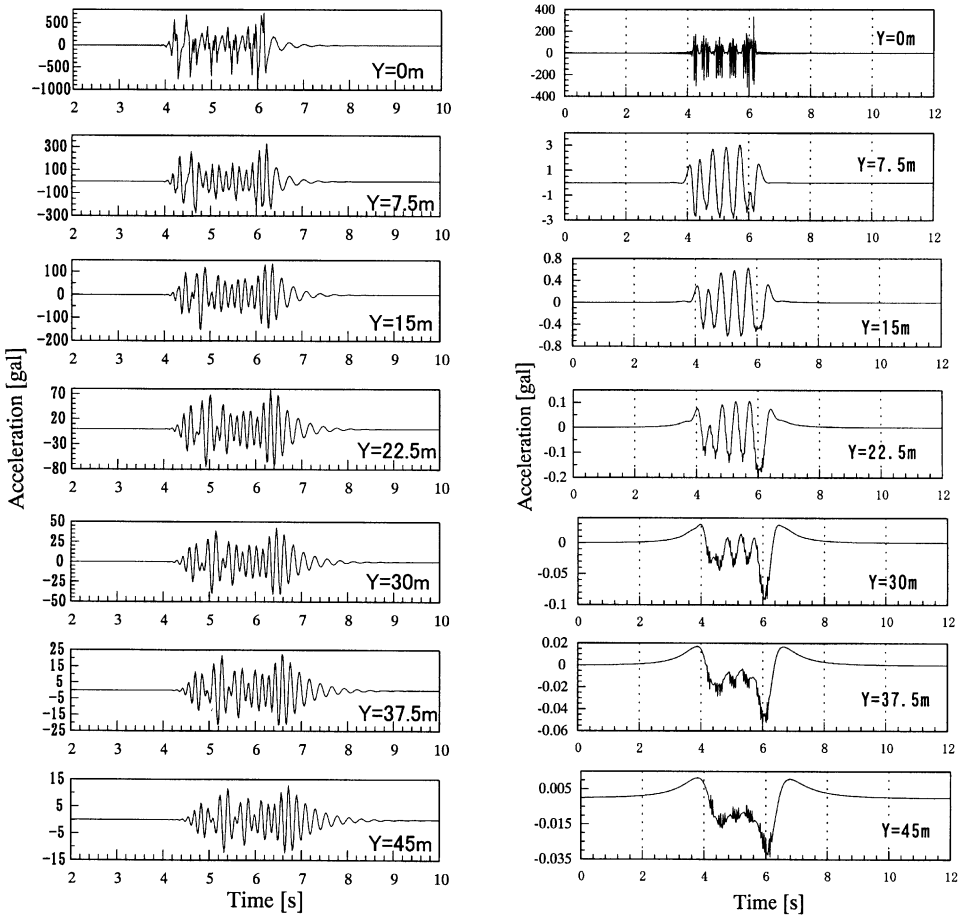

(a) Before soil improvement at the soft portion (b) After soil improvement at the soft portion

Fig. 12. Acceleration response time histories at track and nearby ground surface: (a) before soil improvement at the soft portion; (b) after soil improvement at the soft portion.

referred to for the detailed information. Provided we focus on the response within the WIB extension, we can give an approximate prediction for the response reduction by replacing such inhomogeneous soil layers including cement columns, with the equivalent infinite-horizontally extended homogeneous layers. The soil properties for the soft layers are then increased to be compatible with the WIB installation. In fact, the BANVERKET subsequently took stabilization measures by inserting soil-limestone columns beneath the train track. In this investigation, only by assuming soil improvement based on the above WIB formula, the equivalent layer properties can be calculated as shown in Table 3 [16]. The corresponding computation results are compared with the original responses in Fig. 9 for the high-speed train. The improved soil model in Table 3 has led to a dramatic response reduction. Surprisingly, the response features were brought to similar to those experienced in the quasi-static state for low train speeds so that the wave propagation disappeared as the distance from the track increased.

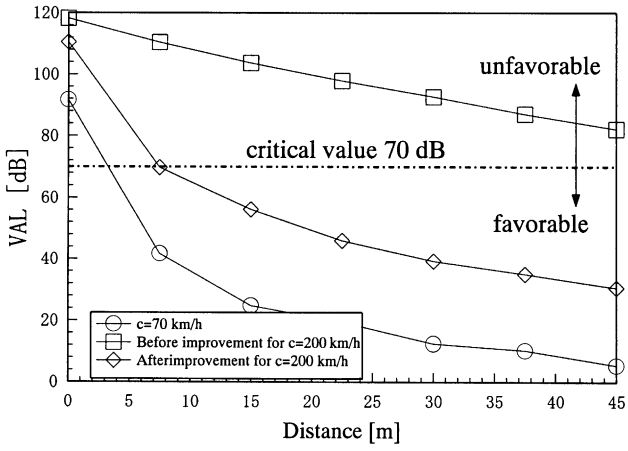

Fig. 13. Vibration Acceleration Level (VAL) attenuation characteristic.

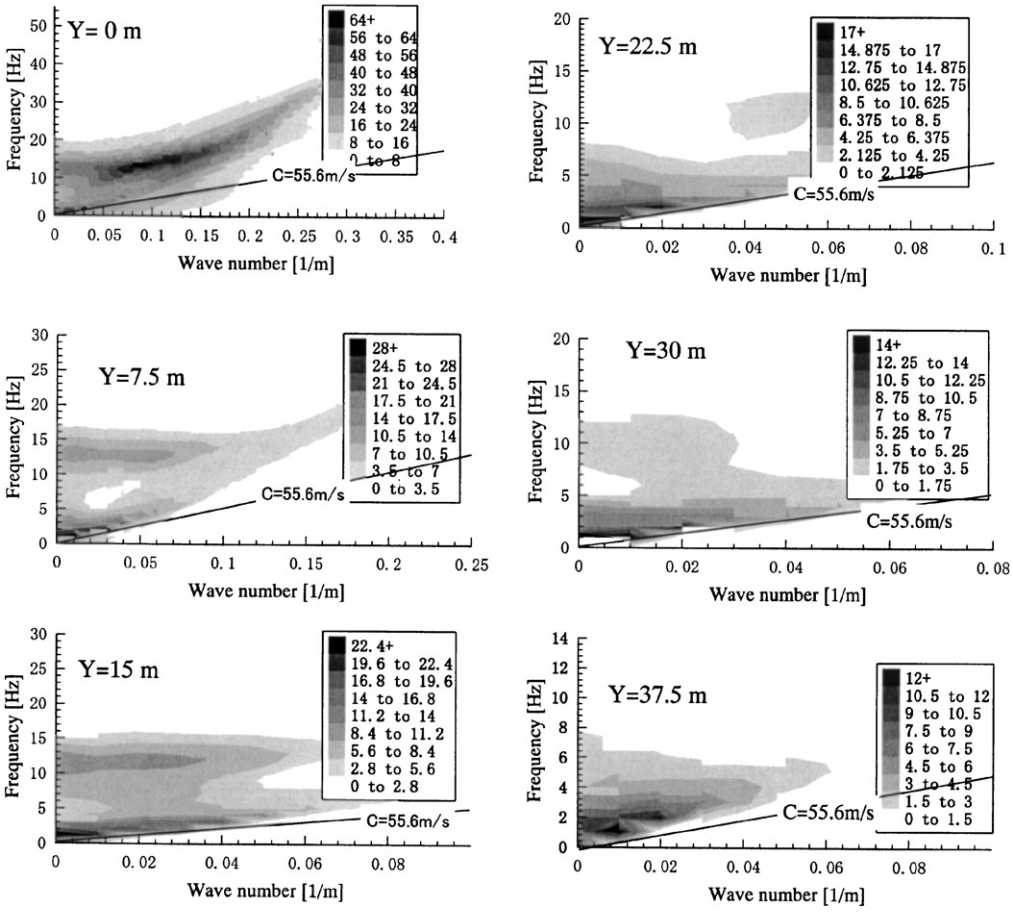

Fig. 14. Frequency–wavenumber spectrum of track and ground surface responses.

In order to confirm the change of wave field before and after the soil improvement, the frequency–wavenumber spectra at certain distances are depicted in Fig. 14. When the train speed line is drawn on the spectra, the zone for the wave propagation has been shifted up so that the speed line is positioned below it as a result. This relation is actually the same for the low train speed so that the soil improvement works better for mitigating the track response and the nearby ground response as well. The response attenuation curves are shown in Fig. 13 for comparison with that before the soil improvement. This suggests that installing the WIB is a very promising method for vibration mitigation.

6. Conclusion

The author has developed a computer simulation method for predicting the vibrations induced by high-speed trains [1]. This paper used the data derived from the operation of the high-speed Swedish the X-2000 train [2] in order to test the validity of the computer simulation and to interpret the observations based on wave propagation theory. It has been proven that moving axle loading and track–ground interaction are primary factors in train-induced vibration, with the sleeper existence being secondary factor.

Through computer simulations the train-induced responses are interpreted in a quasi-static sense for the low speed (70 km/h), while in a dynamic sense for the high speed (200 km/h). At the low speed, the response appears to the axle loads at the instantaneous position so that the moving effect on track is given by the time shifting of the static response configuration accordingly. At the high speed, on the other hand, wave motions occur due to the inertia generated in the track and ground system. The dynamic features were better explained in the Frequency–wavenumber spectra. When the train speed line lies below the ''ridge'' of the spectra, wave propagation does not exist. However, where the speed line intersects the ''ridge'' of the spectrum, an extraordinarily large response results due to the wave field triggered by impulsive axle loading.

The time histories of ground responses are quite different at low and high train speeds. For low speed trains (70 km/h), a clear-cut individual axle load effect appears. However, as the distance from the track to the observation location increases, those corresponding displacements disappear, so that the response turns out to be a smooth long-span displacement owing to the total train weight. The velocity response follows such a change of displacement with distance. A similar trend also holds true for the acceleration response. For high-speed trains (200 km/h), on the other hand, due to a true wave field generation in the track–ground system, the vibration appears in all response quantities at both the track and the nearby ground locations.

In order to give preliminary useful engineering information about applying the vibration mitigation measure, a crude model was investigated in which a soft layer was replaced by an equivalent stiff layer with the WIB installation. The results suggest that a significant response reduction can be expected in the case where the WIB is installed over a substantial area across the transverse section. Also interesting to note is the shift of response features from the dynamic pattern to the quasi-static pattern as a result of the WIB installation. This change was explained by referring to the wave field characteristics.

Acknowledgements

The author would like to thank Mr. Alexander Smekal of the Swedish National Railway (BANVERKET) for providing him with the measurement data and Dr. A.M. Kaynia for additional data. These statistics made possible the present comparison. The various contributions by the participants at the Gotenburg Seminar organized by BANVERKET (2000) in Sweden on "High speed lines on soft ground, dynamic soil–track interaction, ground borne vibrations", were also invaluable in completing this work. Finally, sincere thanks are extended to Mr. M. Kojima for the computation work involved.

References

[1] H. Takemiya, Ground vibrations alongside tracks induced by high-speed trains: prediction amd mitigation, in: V.V. Krylov (Ed.), Noise and Vibration from High-speed Trains, Thomas Telford, London, 2001, pp. 347–393.
[2] BANVERKET, Evaluation and analyses of measurements from the West Coast line, 1997.
[3] J.T. Kenny, Steady-state vibrations of beam on elastic foundation for moving load, Journal of Applied Mechanics 21 (1954) 359–364.
[4] H.A. Dieterman, A.V. Metrikine, Steady-state displacements of a beam on an elastic half-space due to a uniformly moving constant load, European Journal of Mechanics A/Solids 16 (2) (1997) 295–306.
[5] D.C. Gakenheimer, J. Miklowitz, Transient excitation of an elastic half-space by a point load travelling on the surface, Journal of Applied Mechanics, American Society of Mechanical Engineers Series E 36 (3) (1969) 505–515.
[6] V. Krylov, Vibrational impact of high-speed trains. I. Effect of track dynamics, Journal of Acoustical Society of America 100 (5) (1996) 3121–3133.
[7] V. Krylov, Effects of track properties on ground vibrations generated by high-speed trains, Acustica 84 (1998) 78–80.
[8] H. Takemiya, K. Goda, D. Komori, Computer simulation prediction of ground vibration induced by high-speed train running, Proceedings of the Japan Society of Civil Engineers 619 (I-47) (1999) 193–201.
[9] H. Takemiya, Y. Shiotsu, S. Yuasa, Features of ground vibration induced by high-speed train and the counter vibration measure X-WIB, Proceedings of the Japan Society of Civil Engineers 661 (I-53) (2000) 33–42.
[10] H. Takemiya, Simulation of high-speed train induced ground vibration and its mitigation by WIB, Proceedings of the 7th International Congress on Sound and Vibration, Garmisch-Partenkirchen, 2000, pp. 2695–2702.
[11] H. Takemiya, 2.5 D FEM application for predicting ground vibration due to high-speed train and mitigation by WIB, Proceedings of the Eigth Asian-Pacific Conference Structural Engineering & Construction, No. 1070, Singapore, 2001.
[12] H. Grundmann, M. Lieb, E. Trommer, The response of a layered half-space to traffic loads moving along its surface, Archive of Applied Mechanics 69 (1999) 55–67.
[13] X. Sheng, C.J.C. Jones, M. Petyt, Ground vibration generated by a load moving along a railway track, Journal of Sound and Vibration 228 (1) (1999) 129–156.
[14] A.M. Kaynia, C. Madshus, L. Harvik, P. Zackrisson, Ground vibration from high-speed trains: prediction and countermeasure, Journal of Geotechnical and Geoenvironmental Engineering, American Society of Civil Engineers 120 (6) (2000) 531–537.
[15] M. Bouchon, K. Aki, Discrete wave number representation of seismic source wave fields, Bulletin of Seismological Society of America 67 (1977) 259–277.
[16] H. Takemiya, R. Maekawa, M. Kojima, 2.5 D FEM application for predicting ground vibration due to high-speed train and mitigation by WIB procedure, Structural Engineering/Earthquake Engineering, JSCE 710 (I-60) 247–255.